Environmental Engineering and Management Journal

September 2020, Vol. 19, No. 9, 1583-1592
http://www.eemj.icpm.tuiasi.ro/; http://www.eemj.eu

"Gheorghe Asachi" Technical University of Iasi, Romania

RESPONSES OF SHALLOW GROUNDWATER SYSTEM TO DIFFERENT WATER-SAVING PRACTICES IN TYPICAL IRRIGATION AREA IN NORTHWEST CHINA

Fenggang Dai, Xiaogang Fu*, Huanjie Cai[2], Jianqiang He[2]

[1]*Key Laboratory of Water Resources Sustainable Use and Development of Hebei, GEO University of Economics, Shijiazhuang 050031, China*
[2]*Key Laboratory for Agricultural Soil and Water Engineering in Arid Area of Ministry of Education, Northwest A&F University, Yangling 712100, China*

Abstract

The Jinghui Canal Irrigation District (JCID) is a highly productive agricultural area of Shaanxi province, China. Because of severe water scarcity, implementing water-saving renovation practices for agricultural sustainability is necessary. To determine the influence of different water saving practises on the shallow groundwater system in the JCID, ArcGIS and Processing MODFLOW are used to simulate changes in shallow groundwater in the irrigated farmland in this area. The results show that field water-saving measures can reduce 18.5%-33.4% of well irrigation water, and the control effect on groundwater level drawdown is prominent. The shallow groundwater level's declining rate in some areas is increased, owing to the adjustment of the agricultural planting structure. Moreover, the spatiotemporal distributions of water and soil resources do not reasonably match, which offsets the active impact of water-saving renovation in the mitigation of falling groundwater tables. The groundwater's annual average decline rate has increased from 0.535 m year^{-1} during 1981-1997 to 0.734 m year^{-1} during 2000-2014. The groundwater cone of depression shows a continuous expanding tendency. The area in which the groundwater depth is larger than 13 m has increased from 358.56 km^2 in September 1997 to 612.92 km^2 in September 2014. However, successful agricultural water-saving renovation requires a practical feasibility of water-saving projects, in addition to an appropriate planting structure, strong bearing capacity of farmers, water-saving propaganda, and policy implementation of agricultural subsidy and water resource management.

Key words: groundwater level, Jinghui canal irrigation district, processing MODFLOW for windows, water-saving renovation

Received: October, 2019; Revised final: March, 2020; Accepted: April, 2020; Published in final edited form: September, 2020

1. Introduction

Water resource shortage is one of the most important factors constraining the long-term economic development in arid–semiarid areas in China (Li et al., 2009; Liu et al., 2020; Odeh and Mohammad, 2020). In the Guanzhong Plain in northern China, water per capita is only approximately 446 m^3 annually (Wang et al., 2002), which is far lower than the 1000 m^3 year^{-1} per capita benchmark line of water scarcity recognized by the United Nations Educational, Scientific and Cultural Organization (UNESCO). A rapid groundwater-table decline caused by the overpumping of groundwater for irrigation occurs in the Jinghui Canal Irrigation District (JCID) (Liu and Zhu , 2011), which is estimated to be the largest groundwater drawdown area in the Guanzhong Plain. In most regions of the JCID, groundwater is declining at a rate of 0.734 m·year^{-1} (Liu., 2005). Agricultural water use has been recognized as the largest water consumer, accounting for 80% of the total water use, and is the major contributor to the local groundwater decline (Geng 2020; Zhao et al., 2009). Although the annual mean precipitation in this region was only

* Author to whom all correspondence should be addressed: e-mail: fuxiaogang@hgu.edu.cn; Phone: +86 13315457630

approximately 530 mm, a substantial amount of the agricultural water supply could be satisfied by a widely distributed irrigation canal network that relies partly on the intensive use of groundwater. Winter wheat and summer maize are the two staple crops in this region, accounting for 85% and 65% of the total crops cultivated in 2000, respectively. The long-term excessive extraction of groundwater and poor irrigation/drainage management practices in the irrigation districts have caused environmental geological disasters, such as severe groundwater declines and ground fissures. Since 2001, diverse and effective water-saving measures have been considered and have gradually been implemented in irrigation districts to improve the efficiency of both farm water use and canal water conveyance. Water-saving measures for improving water conveyance include the lining of canals, upgrading of hydraulic control equipments, and canal water delivery management. Measures for improving farm water use efficiency include optimized irrigation regime, land leveling of irrigated farm, and improved furrow irrigation systems. Monitoring and evaluation networks have been constructed for management system reform in the Guanzhong Canal Irrigation District (Wang et al., 2003).

Efficient irrigation systems can reduce both evaporation and deep percolation (Abu-Awwad, 1999; Bietresato and Mazzetto, 2020; Vovna et al., 2019); however, the deep percolation rate of irrigated water returning to the groundwater aquifer can only be estimated (Rushton, 2010; Xiao et al.,, 2014). Systems with higher efficiency would result in less water returning to the aquifer (Kushwaha et al., 2009; Wang and Huang, 2011). In this study, the JCID was selected as a typical example because of the cooperation of the Jinghuiqu Administration of Shaanxi Province and because adequate data were available for the current study. In particular, the JCID is a representative irrigation district of wells combined with canals. More research has been concentrated on groundwater quality assessment in the basin scale (Maheswaran and Elangovan, 2010).

Groundwater models are generally accepted to be appropriate tools for assessing the effects of future human activities on groundwater dynamics (Clemo, 2005; Hanson et al., 2010; Fu et al., 2018; Geng et al., 2013; Zhang et al., 2019). However, groundwater models require a large amount of good-quality data on hydrogeological settings, which include the boundary conditions of the aquifer system, main hydrogeological parameters of each aquifer layer, and long-term dynamics of groundwater levels. Because the parameters vary in both time and space, coupling geographic information system (GIS) technology with a groundwater model for hydrogeological system characterization and conceptualization is necessary (Pathak and Hiratsuka, 2011; Xu et al., 2009; Xu et al., 2011). Studies on the response of shallow groundwater system to water-saving renovation in a large-scale irrigation district are comparably few. Thus, ArcGIS 9.3 and Processing MODFLOW for Windows (PMWIN) were integrated with JCID research as an example study with the objectives as follows: (1) to evaluate and predict the influence of various water-saving practices on the spatiotemporal dynamics of the shallow groundwater table and (2) to provide a scientific basis for the reasonable evaluation of the groundwater environment in response to the implementation of water-saving irrigation planning. The proposed method/model is successfully tested for the 1180 km^2 Jinghui Irrigation District, which is in the center of the Guanzhong Pain.

2. Material and methods

2.1. Example site description

The JCID (34° 25' 20"-34° 41' 40" N; 108° 34' 34"-109° 21' 35" E; 350-450 m), located in the center of the Guanzhong Plain, Shaanxi Province, China, is a large (II)-type irrigation project with artesian water from the Jing River with an approximate length (east to west) of 70 km, width (north to south) of 20 km, and total area of 1180 km^2 (Fig. 1). The terrain slants from northwest to southeast with a slope of 1/300-1/600. This area is a typical northern plain irrigation region. The average annual rainfall is 535 mm, 60% of which is concentrated in June-September, and the average annual evaporation is 1212 mm, which classifies the region as a semi humid area (Fig. 2).

This region belongs to the Weihe Basin water system of the Yellow River, of which the major surface rivers are the Jing, Qingyuhe, and Shichuanhe rivers. The main irrigation water source is the region’s largest river, the Jing River, with a length of 455 km and a drainage area of 43.126 km^2 over the Zhengguo canal head of Zhangjiashan. The JCID includes the counties of Jing Yang, Sanyuan, Gao Ling, Lintong, Yanliang, and Fuping and the cities of Xianyang, Xi’an, and Weinan. The designed irrigation area of the district is approximately 9.7×10^2 km^2, and the effective irrigation area is 9×10^2 km^2. Although the irrigated land area covers only 2.4% of the size of the province, it produces approximately 5.7% of the province’s grain. This area is a major grain producer of Shaanxi Province and a major supplier of other agricultural products, such as vegetables and fruits, to Xianyang and Xi’an Groundwater includes phreatic and confined waters.The phreatic water in the Quaternary alluvium in the Holocene is relatively shallow as a main irrigation extracting aquifer and is widely distributed in the region. In the first and second terrace areas in the river floodplain, the depth is 6-16 m. In the third terrace region of the Weihe and Jing rivers, the depth is generally 20-40 m, and the aquifer is composed mainly of Pleistocene alluvial loam, clay, sand, and gravel layers with a thickness of 13-80 m.

2.2. Conceptual hydrogeological model

The study area is adjacent to the Loess Plateau in the north and is surrounded by the Jing, Wei, and ShiChuan rivers at the west, south, and east, respectively.

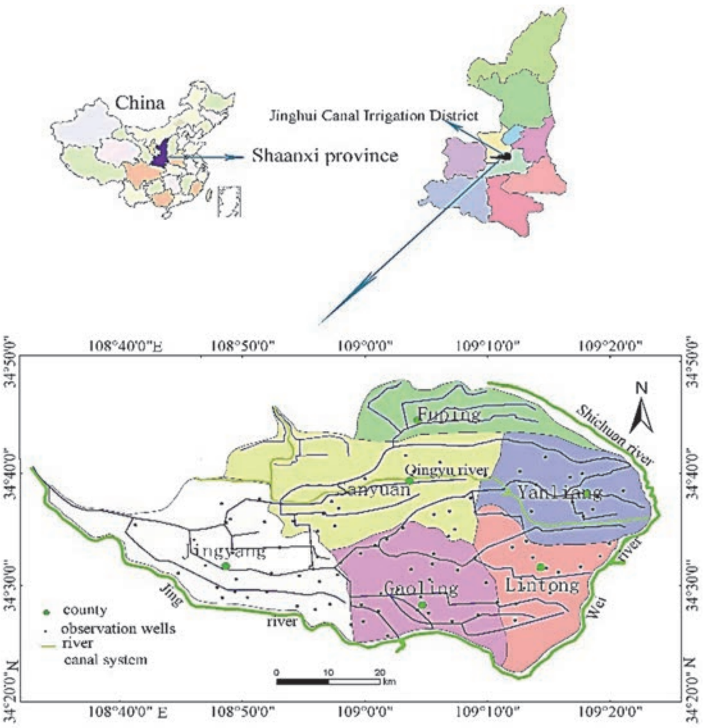

Fig. 1. Location of the Jinghui canal irrigation district in China

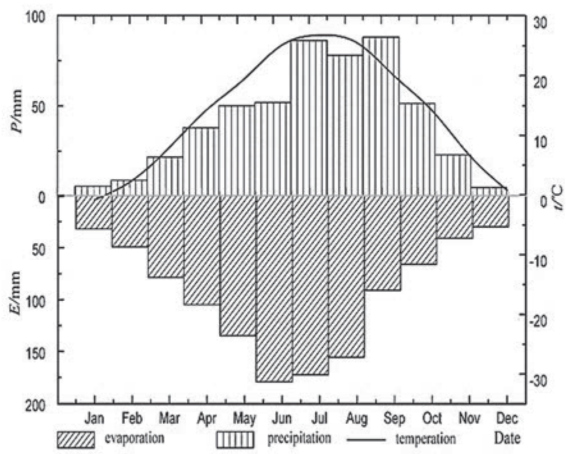

Fig. 2. Main meteorological elements in the irrigation districts (the meteorological data comes from Jinghui Canal Management Bureau of Shaanxi Province)

The Qingyu River runs from west to east in the northern irrigation area, which is a complete hydrogeological unit. Using 13 drilling histograms (LI2, H19, X16, L8, H11, S4, G4, B8, B2, B3, B5, J18, and J85) and associated hydrogeological profile information, a three-dimensional (3D) irrigation aquifer distribution model was created (Fig. 3) to reveal the space structure of the aquifer system in the irrigation area and to lay a foundation for the groundwater simulation model (Borgia et al., 2011; Huo et al., 2012; Lin et al., 2010).

The aquifer contains a very thick late Quaternary (late Pleistocene and Holocene (Q_4+Q_3)) layer of coarse sand and gravel sand, and the central part is mainly mid-Pleistocene series Q_2 clayey silt and clay sand. According to the 3D irrigation aquifer distribution model, the hydrogeology units in the irrigation area are generalized as the upper unconfined aquifer and the lower equivalent confined aquifer.

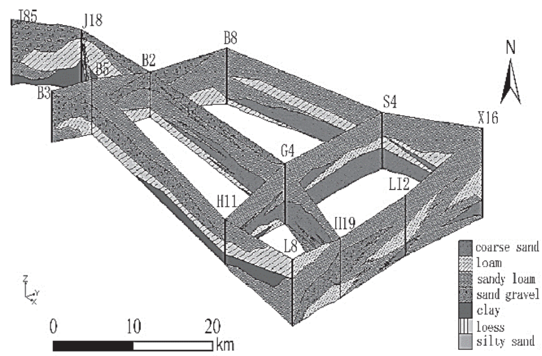

Fig. 3. Three-dimensional aquifer structure of the irrigation district

The two model layers were separated by an equivalent semi pervious layer (Barazzuoli et al., 2008). The confined aquifer is generally buried at a depth of 100 m. It is suitable for supplying further water resource and generally is not used as an irrigation water source. The phreatic aquifer is generally stored in the Quaternary Holocene alluvial layers, which are shallowly buried, accessible, and widely distributed. The main supply source includes the vertical infiltration of the precipitation and leakage recharge of the irrigation canal system. The secondary source is a supplying the horizontal direction and the water infiltration supply of the riverbank. In comparison, the latter recharge is low. The phreatic water is excreted through runoff to the Jing, Wei, and Qingyu rivers. Only in the midstream and downstream of the irrigation area, during the flood season with a high water level, the phreatic water produces a short supply from the rivers along the edges of the Wei and Jing rivers, the water quantity is few. The northwestern loess border of the irrigation area, which accepts the lateral flow of tableland supplies, is set as the third boundary or the given flow boundary (Bumb et al., 1997); the eastern, southern, and central regions of the Wei, Jing, and Qingyu rivers are the main horizontal excretion zones and are set as the river boundaries.

2.3. Groundwater model

According to the hydrogeological conceptual model and its available materials, the study area is generalized as a quasi-3D flow groundwater aquifer system that can be described by a differential equation and definite solution conditions (Brunner et al., 2010; Doble et al., 2009): The equation for shallow unconfined aquifer is as Eqs. (1-2) etc.

$$\begin{cases} \frac{\partial}{\partial x}\left[K(H_1-B)\frac{\partial H_1}{\partial x}\right]+\frac{\partial}{\partial y}\left[K(H_1-B)\frac{\partial H_1}{\partial y}\right]+W_1+\varepsilon+\frac{K'}{M'}(H_2-H_1)=S_y\frac{\partial H_1}{\partial t}, (x,y)\in G, t>0 \\ H_1(x,y,t)=H_{10}(x,y), \quad (x,y)\in G, t=0 \\ K\left(H_1-B\right)\frac{\partial H_1}{\partial n}\bigg|_{\Gamma_2}=q(x,y,t), \quad (x,y)\in \Gamma_2, t>0 \end{cases} \tag{1}$$

deep confined aquifer:

$$\begin{cases} \frac{\partial}{\partial x}\left[T_2\frac{\partial H_2}{\partial x}\right]+\frac{\partial}{\partial y}\left[T_2\frac{\partial H_2}{\partial y}\right]+W_2+\frac{K'}{M'}(H_1-H_2)=S_2\frac{\partial H_2}{\partial t}, (x,y)\in G, t>0 \\ H_2(x,y,t)=H_{20}(x,y) \quad (x,y)\in G, t=0 \\ \mathrm{T}_2\frac{\partial H_2}{\partial n}\bigg|_{\Gamma_2}=q_{2b}, \quad (x,y)\in \Gamma_2, t>0 \end{cases} \tag{2}$$

where: K is the permeability coefficient of the phreatic aquifer (m/d); H_1 (x, y, t) and H_2 (x, y, t) are water levels at different times in the area (m); B (x, y) is the bottom elevation of the unconfined aquifer (m); H_{10} (x, y) and H_{20} (x, y) are the initial water head of the phreatic aquifer and confined aquifer (m), respectively; S_y is the specific yield of the unconfined aquifer; S_2 is the storage coefficient of the confined aquifer; K' and M' are the infiltration coefficient (M/d) and thickness (m) of the semi pervious layer, respectively; T_2 is the transmissivity of the confined aquifer (m^2/d); T is the calculating time (d); W_1 and W_2 are the source-sink terms of the aquifer water in the vertical supplies (m^3/d); ε is the evaporation strength of the unconfined aquifer (m); G is the calculation area; Γ_2 is the third-class boundary; and Q (x, y, t) is the unit area flow of the third-class boundary (m^3/d/m^2).

2.4. Groundwater numerical simulation model

The PMWIN simulation analysis software was adopted to solve the definite problem of groundwater movement (Kinzelbach et al., 1992). PMWIN is an application software developed by the United States Geological Survey (USGS) for the simulation and forecasting of groundwater systems. This program uses MODFLOW as the core and can be used to examine 3D groundwater models. The model calculation scope is from the Loess Plateau to the Wei River, with west and east boundary lines of 19,276 km and 19,351 km, respectively. Excluding the area that is not part of the modeling calculation scope, the total effective area for modeling was 1,225 km^2. The mesh size of the model was 500 m × 500 m, and the time step of time was a natural month division.

(1) Hydrogeological parameters. According to the hydrogeological conditions and the Quaternary distribution of loose sediment, the simulated region was divided into 11 parameter areas. The initial hydrogeological parameters (Table 1) were directly obtained from a pumping test and were used as the benchmark reference parameters. With the analogy method and the reference of other single pumping test data, the initial value parameters of the other partition were estimated for model correction in the confirmation stage. Four parameters (***K, S*$_y$**, ***T***, ***S***) are the key parameters, so it's just listed in the Table 1.

Table 1. Hydrogeology parameters

Partition parameter	*K/(m/d)*	S_y	*T/(m^2·d^{-1})*	*S*
I	100	0.12	2050	0.002
II	65	0.1	2000	0.0018
III	40	0.08	1000	0.0015
IV	35	0.07	450	0.0012
V	45	0.06	500	0.0011
VI	20	0.03	400	0.0012
VII	10	0.05	300	0.001
VIII	75	0.06	400	0.001
IX	8	0.03	200	0.0009
X	4	0.04	120	0.001
XI	2	0.04	100	0.0007

(2) Source and sink. The supplies mainly included precipitation infiltration recharge and irrigation water infiltration recharge, accounting for more than 90% of total recharge (Xie and Yang, 2013). With the comprehensive consideration of the precipitation, soil type, underlying surface, and burial depth of the underground water level of the unsaturated zone, the rainfall infiltration recharge coefficient was determined by the rainfall data (1953-2000) in the irrigation area, and the statistical analysis of the long-term observation data of 93 groundwater wells (1988-2000) was performed (Table 2). All planar and linear sources and sinks of data were then converted to strength form. The superposition calculation was used for the conversion into single-grid strength, and the obtained values were guided into the models through recharge and well modules.

Table 2. Precipitation infiltration coefficient-α and irrigation infiltration coefficient-β

Depth interval /m	<1	1–3	3–5	5–7	7–10	>10
α	0.32	0.26	0.22	0.19	0.15	0.10
β	0.48	0.35	0.30	0.24	0.18	0.09

The evapotranspiration (EVT) of the MODFLOW subroutine is a linear vaporization model. The relationship between shallow groundwater evaporation and burial depth is nonlinear, and the evaporation factors account for a large portion in the groundwater equilibrium analysis. Moreover, the calculation error of the linear model evaporation is higher. In this study, the Аверьянов, Г.В nonlinear formula was used in the EVT evaporation module, rather than the linear formula for calculating the evaporation capacity (Ajami et al., 2012). The source code was rewritten using Visual Basic 6.0 in the EVT module. The nonlinear formulas are as follows (Eq. 3):

$$\begin{cases} R_{ETi,j} = R_{ETMi,j}, & h_{i,j,k} > h_{s,j,k} \\ R_{ETi,j} = R_{ETMi,j}\left(1 - \dfrac{h_{s,j,k} - h_{i,j,k}}{d_{i,j}}\right)^{m}, & h_{s,j,k} - d_{i,j} < h_{i,j,k} < h_{s,j,k} \\ R_{ETi,j} = 0, & h_{i,j,k} < h_{s,j,k} - d_{i,j} \end{cases} \tag{3}$$

where: $RETM_{i,j}$ is the underground water evaporation strength, which depends on local meteorological conditions (m); $RET_{i,j}$ is the phreatic evaporation strength, which changes by month with unit area and unit time water volume (m); $H_{i,j,k}$ is the unit water head or underground water level (m); $H_{s,j,k}$ is the evaporation interface elevation (m); $d_{i,j}$ is the evaporation limit depth of groundwater (m) relative to lithologic features; and *m* is a dimensionless index, taken as approximately 2 for the region.

A comparison of RET accuracy before and after adjustment showed strong improvement. Moreover, the superposition of the groundwater-table calculation value under the stable flow simulation showed a good fit, and the groundwater depth lines were united as the virtual evaporation interface elevation. This elevation replaced the practical evaporation interface elevation and was imported into the EVT modules. Debugging and fitting were repeated to detect small differences from the virtual evaporation interface and the calculation of the water level elevation; the groundwater depth was essentially consistent. Such measures were performed to avoid an inconsistent regional distribution of the actual evaporation and the simulation value caused by the fitting error of the groundwater flow field and to improve the simulation degree of water resources.

2.5. Model calibration and validation

The model identification period was set from January 1996 to December 1998, and the model validation period was from January 1999 to December 2000. The monthly average groundwater level data of 93 long-term observation wells at 14 stations of Shiqiao, Jingyang, Sanqu, Yangfu, Sanyuan, Pengli, Gaoling, Xizhang, Zhangbu, Pixi, Xinshi, Liyang, Loudi, and Xumu were used in model identification and validation. The flow field in January 1996 was taken as the initial water head. The hydrogeology parameters were manually adjusted by using the forecast correction method (Jhorar et al., 2011; Praveena and Aris, 2010). The flow field and the actual simulation flow field were similar, and the simulation value and groundwater dynamics were essentially equal. According to the water level materials of the 93 long-term observation wells, 44 observation holes were selected for simulation after eliminating the materials of imperfect observation hole parts. The statistical absolute error had an average of 1.36 m. The mean absolute error was less than 0.5 m in 23 observation holes for a total of 52.3%; those between 0.5 m and 1 m and more than 1 m were noted in 16 and 5 observation holes for totals of 36.4% and 11.3%, respectively. Fig. 4 shows the fitting of 6 typical observation holes. By calculating the flow field and the variation of the line fitting process, the simulation results are obtained to reflect the underground water flow field characteristics in the irrigation area, which can be used for the numerical calculation of groundwater (Fig. 4).

2.6. Scenario simulations with groundwater model

Four different scenarios of the planning level years in 1997, 2005, 2010, and 2013 were simulated with the goal of remaining consistent with water-saving plans (Tables 3 -4). Through groundwater water modeling, the underground water table and burial depth of the reconstruction project implemented in the years before 1997 were calculated, as was the water conservation project implemented after 2005 and 2010. Moreover, the analysis and prediction of underground water level and burial depth in 2014 and the influence of the shallow groundwater system in response to water-saving irrigation transformation were compared before and after implementation of the water-saving reconstruction project.

3. Results and discussion

3.1. Results of model calibration and validation

Comparisons between the simulated and observed values of groundwater tables of the typical observation wells are presented in Fig. 4 to show the results of model calibration and validation. With the estimated hydrogeological parameters, the model can correctly simulate the groundwater system. For model calibration, the simulated and observed values were consistent; a difference of only 5% was noted in the simulated values for the typical observation wells. The groundwater level that was simulated agreed well with the level that was observed. The observed and simulated groundwater levels were compared through a linear regression forced to the origin; the respective coefficients of regression and determination were b=1.0 and R^2=0.99.

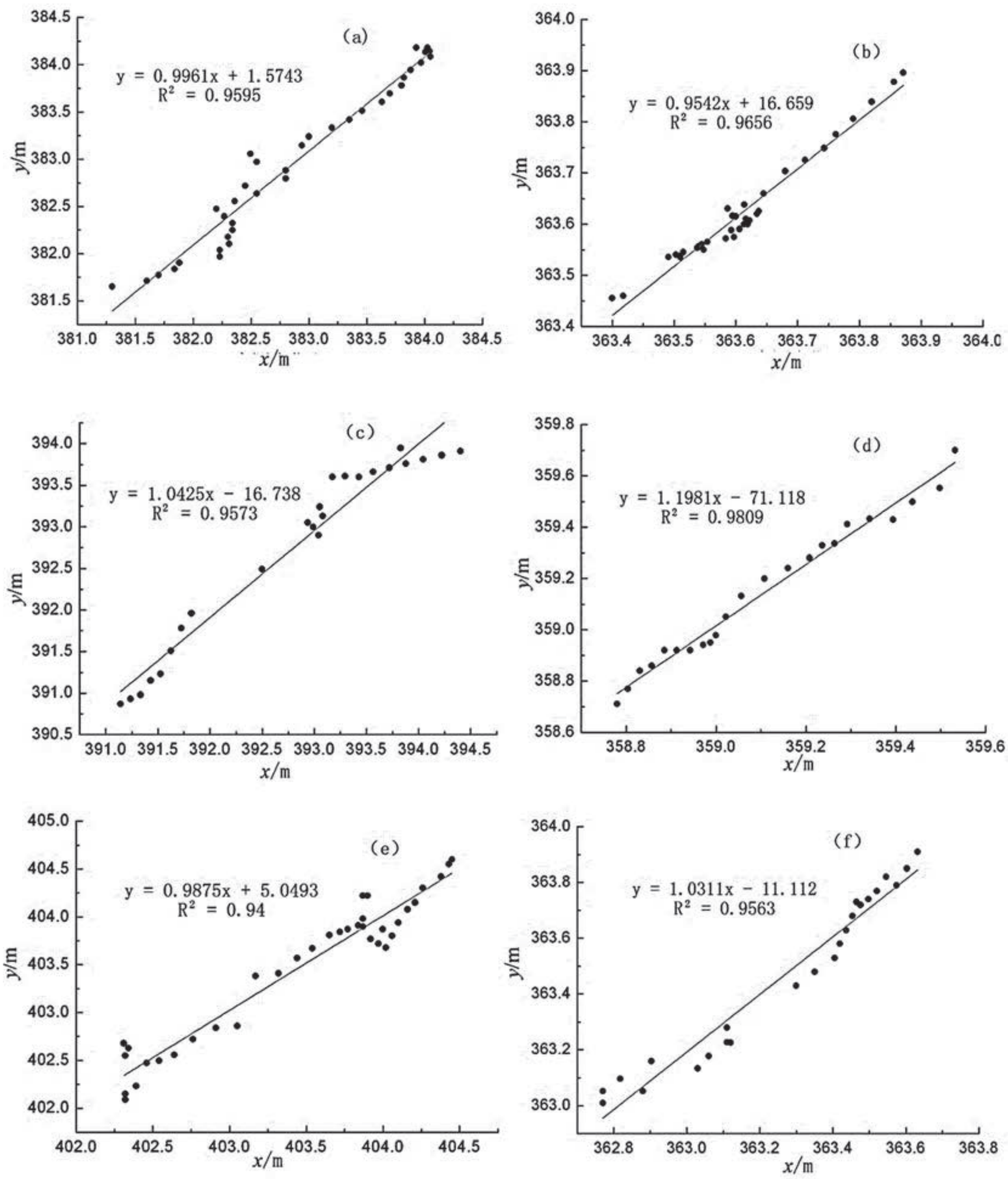

Fig. 4. Groundwater level fitting of typical observation wells: (a) represent stations of Shiqiao, (b) represent stations of Jingyang, (c) represent stations of Yangfu, (d) represent stations of Gaoling, (e) represent stations of Xinshi, (f) represent stations of Loudi

Table 3. Scene settings of water-saving transformation in the irrigation district

Simulation scene		1	2	3	4	5	6	7	8
Channel water saving	x_1	0.395	0.395	0.395	0.75	0.75	0.75	1	1
	x_2	0.42	0.42	0.42	0.8	0.8	0.8	1	1
	x_3	0.574	0.574	0.574	0.645	0.645	0.645	0.671	0.671
Field water saving	x_4	17666.76	42000.21	42000.21	42000.21	53333.6	53333.6	53333.6	60000.3
	x_5	0	4666.69	4666.69	4666.69	8666.71	8666.71	8666.71	10000.05
	x_6	0	2000.01	2000.01	2000.01	4000.02	4000.02	4000.02	5333.36
	x_7	0	8666.71	8666.71	8666.71	11666.73	11666.73	11666.73	13333.4
	x_8	0.9	0.9	0.9	0.9	0.92	0.92	0.92	0.93
Agricultural structure	x_9	62206.98	62206.98	66867	66867	66867	63266.98	63266.98	63266.98
	x_{10}	5333.36	5333.36	8466.71	8466.71	8466.71	12400.06	12400.06	12400.06
	x_{11}	6920.03	6920.03	7866.71	7866.71	7866.71	9133.38	9133.38	9133.38
	x_{12}	3420.02	3420.02	6000.03	6000.03	6000.03	6533.37	6533.37	6533.37

Table 4. Parameters of scene settings of water-saving transformation in the irrigation district

Parameter	***Unit***	***Definition***
x_1	--	Arterial lining rate
x_2	--	Canal lining rate
x_3	--	Water utilization efficiency of canal system
x_4	hm^2	Border irrigation area
x_5	hm^2	Sprinkling irrigation area
x_6	hm^2	Microirrigation area
x_7	hm^2	Low-pressure pipe irrigation area
x_8	--	Field water utilization coefficient
x_9	hm^2	Food crops in irrigation area
x_{10}	hm^2	Vegetable irrigation area
x_{11}	hm^2	Orchard irrigation area
X_{12}	hm^2	Other economic crop area

For model validation, the simulated daily groundwater levels of six observation wells (a, b, c, d, e, and f) were selected (Fig.4). Observation wells a and b were located in the north area with sandy loam and c and d were in the south area with loamy soil. The fluctuations of simulated groundwater levels agreed reasonably with the observation data. However, some discrepancy remained between the simulated groundwater levels and the observations. When compared with the observed values, the simulated groundwater levels at observation well e were slightly lower, whereas those at well d were higher. These results imply that uncertainties may be imposed by model parameters, model structure, and model input.

In general, the calibrated groundwater model can be concluded to accurately simulate changes in the groundwater table in the JCID under various conditions of different water saving practices.

3.2. Comparisons among various simulation scenes of water-saving transformation

Eight scenes of water-saving transformation in the JCID were simulated and compared to determine the responses of the shallow groundwater system to the different water saving practices (F.5). Notably, the groundwater flow distribution is to a large extent closely related to the water-saving measures of the JCID mentioned previously.

When no irrigation or a small amount of irrigation was applied during the rainy season, some moderate groundwater-table changes arose prior to the water-saving transformation in the JCID (Figs. 5a, 5b, 5c, and 5d). Then, more considerable changes in the groundwater tables occurred after the implementation of the water-saving measures. For the local areas of Jingyang and Gaoling, the cumulative decline of the groundwater level was 15 m. Therefore, a guideline for water conservation planning is the reasonable use of limited water resources to avoid the continuous decline of groundwater levels.

Notably, when the water-saving measures were applied, e.g., in the 2-, 5- actual scenes, an expanding trend of groundwater funnel appeared in a very short period or completely disappeared in some areas at the later stages. However, the field water-saving measures reduced 18.5%-33.4% of the well irrigation water usage. In the 5- actual scene, a short but severe water-table decline occurred after the application of border irrigation and micro irrigation, whereas the decline in the sprinkler irrigation area increased (Fig. 6).

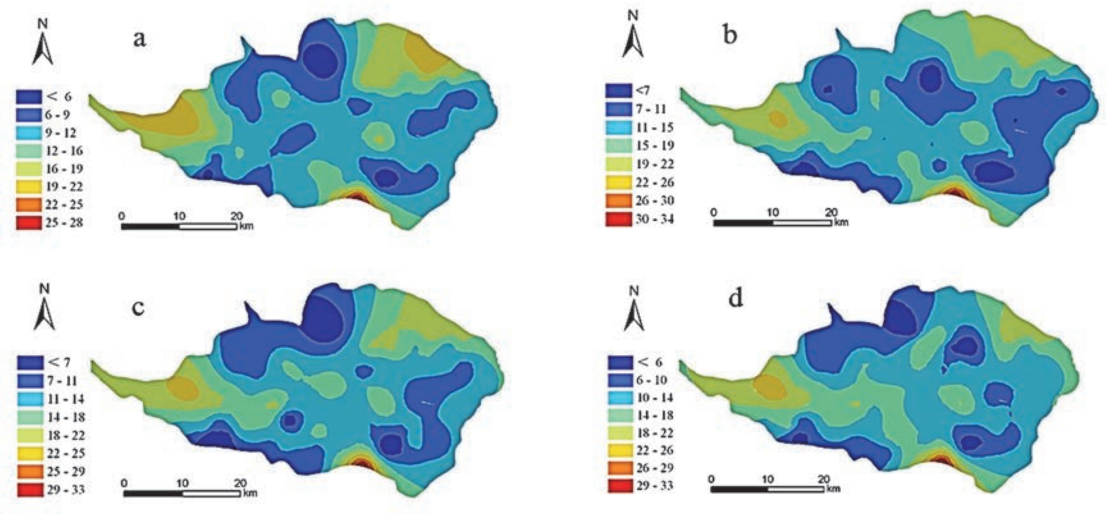

Fig. 5. Various scenes of space distribution of groundwater depth in the irrigation district: a- represent stations of Shiqiao, b-represent stations of Jingyang, c-represent stations of Yangfu, d-represent stations of Gaoling

These results may explain why the areas with the groundwater burial depth between 8 m and 13 m in the 5- actual scene were approximately 6.4% lower than those in the 2- actual scene. A comparison of the areas of different groundwater burial depths in the 2- and 5- actual scenes shown in Figs. 6e, 6f, respectively, revealed that the groundwater table may be heavily influenced by the field water-saving measures implemented in the areas with an expanding trend of groundwater funnel.

The curves of the water table for groundwater (Figs. 6f, 6g, 6g) indicated that the channel water saving had an impact on groundwater flow distribution. A comparison of the 1- actual scene and the 6- simulation scene revealed that the areas in which the groundwater burial depth was less than 8 m increased by 17.2%; those of 8-13 m decreased by 31.5%. A comparison of 3- and 4- simulation scenes revealed a 2.3% increase in the areas in which the groundwater burial depth was less than 8 m and 2.1% decrease in the areas in which the depth was 8-13 m. Analysis of 1- and 7- actual scenes revealed a 10.5% increase in the areas in which the groundwater depth was less than 8 m and 18.5% decrease in the areas in which the depth was 18-23 m. Canal water-saving engineering measures decreased channel leakage, which reduced the groundwater recharge. However, these measures improved the use coefficient of the canal water, reducing the well irrigation water. Therefore, the underground water level drop had a certain inhibitory effect. Moreover, a comparative analysis of 1- and 8- actual scenes led to the speculation that the unreasonable agricultural structure contributed to the underground water level decrease, and an expanding trend of groundwater funnel appeared. The areas in which the burial depth was more than 28 m increased 7.6 times; those of 23-28 m increased 4.76 times. A comparison of 3- and 7- simulation scenes revealed that the areas in which the groundwater burial depth was more than 28 m increased 4.78 times; those of 23-28 m increased 2.99 times. The analysis of 2- and 6- simulation scenes revealed that the areas in which the groundwater burial depth was more than 28 m increased 2.13 times; those of 23-28 m increased 2.15 times.

3.3. Effect on groundwater recovery

For the study area and the most extensive Quaternary Holocene alluvium, approximately 70% of total groundwater use is in the agricultural sector. Industrial and domestic sectors account for approximately 20% and 10% of the total groundwater use, respectively. Per capita water availability in the area is only 446 m^3 per annum, which is 641 m^3 less than the 1000 m^3 $year^{-1}$ benchmark for semiarid regions (Berkoff, 2003). Hence, the water-saving measures in the region should focus on the agricultural sector, which uses the largest amount of groundwater.

MODFLOW estimated that the agricultural water reduction under the equilibrium condition is 29.8%, which is equivalent to 136.95 mm of irrigation water for the 1180 km^2 study area(Table 5). This result implies that the water-saving transformation should be reduced by 136.95 mm to prevent further groundwater storage depletion in the study area. Further analysis shows that a 136.95 mm reduction in the annual irrigation pumping of groundwater relates to an annual groundwater storage gain equivalent to 0.35 m of the aquifer thickness.

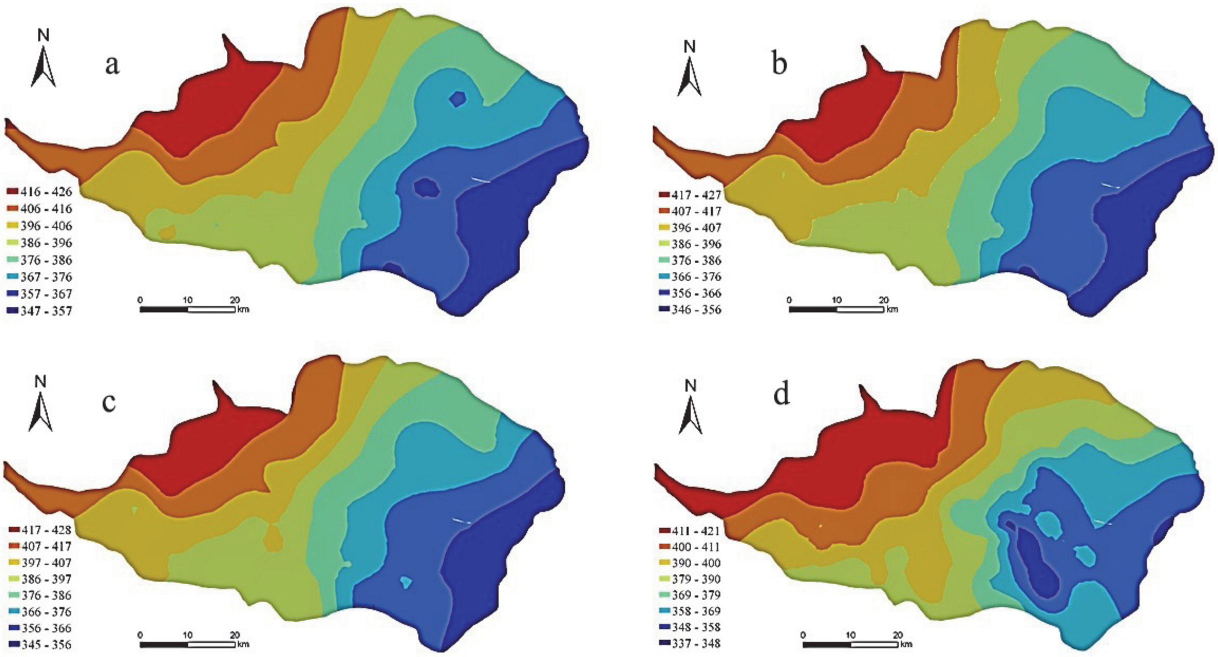

Fig. 6. Various scenes of space distribution of groundwater levels in the irrigation district: a-represent stations of Xinshi, b-represent stations of Loudi, c-represent stations of Pixi, d-represent stations of Xumu

However, maintaining groundwater levels at the equilibrium condition is not acceptable because the cumulative decline of average groundwater levels for 1981-2003 is 11.9 m below the land surface. Hence, to restore groundwater levels to the predevelopment hydrologic conditions of 1981, effective agricultural water-saving measures beyond the equilibrium condition are necessary.

Irrigation is the main method for improving agricultural production in the area because of the semiarid climate. However, farmers are generally inclined to overirrigate because many do not have the required knowledge regarding the water-saving measures of irrigation. This inadequate practice wastes a large amount of the limited water resources, while a much smaller amount of irrigation water could yield similar productivity.

Table 5. Various groundwater depth distributions with water-saving renovation in the irrigation district/km^2

Burial depth/m	***<8***	***8–13***	***13–18***	***18–23***	***23–28***	***>28***
1	110.31	736.21	248.25	123.53	5.08	1.69
2	115.35	626.32	335.26	136.58	8.28	3.28
3	120.59	552.09	385.81	152.15	10.16	4.27
4	123.35	540.25	405.18	140.56	10.86	4.87
5	126.48	516.84	432.05	132.2	11.66	5.84
6	129.26	504.38	435.03	120.08	26.05	10.27
7	139.76	472.39	439.88	107.71	40.63	24.7
8	165.25	468.28	442.26	105.35	29.28	14.65

4. Conclusions

The development of process-based groundwater simulation models has provided opportunities for conducting a comprehensive analysis of groundwater recovery based on water-saving transformation. Such analysis can be used to address questions related to the effects of different watersaving practises on groundwater systems in future.

In this study, ArcGIS 9.3 and a groundwater model were integrated to simulate groundwater recovery in the JCID. The model has been calibrated for 1981-1989 and validated for 1990-2001 by using a large number of field measurement data. Through a series of model simulation analyses based on the results of field experiments, some conclusions related to groundwater recovery in the JCID have been drawn.

The implementation of the field water-saving measures can reduce 18.5%-33.4% of the well irrigation water, which indicates an obvious control effect on groundwater level drawdown.

Moreover, channel water-saving measures have an impact on the groundwater flow distribution. Channel water-saving engineering measures decrease channel leakage, which increases the water use coefficient by 16.9%. In addition, groundwater exploitation is reduced.

Finally, the correlation of the agriculture planting structure and spatiotemporal distributions of water and soil resources are not reasonable, which offsets the slow decrease effect of groundwater levels on water-saving transformation. In addition, the groundwater drop funnel trend is increased.

Apart from the unreasonable agricultural structure, channel water-saving engineering is also responsible for a reduction in the groundwater exploitation, although the effect is somewhat limited. The field water-saving measures are expected to be gradually accepted voluntarily. With the economic and social development of the irrigation area and given the environmental, ecological, and socioeconomic benefits of groundwater restoration, farmers have a certain incentive to invest in small water-saving projects. However, the actions of farmers alone are insufficient. Water-saving incentives and the policy regulation and enforcement of the water resource management are required to resuscitate the degrading ecology and environment in these areas, and such measures must pay equal attention to water-transferring projects from the water-rich south to the water-poor north.

Acknowledgements

We are grateful to “12th Five-Year” National Science and Technology Support Program (No. 2011BAD29B01), The key project of the Department of Education in Hebei province (No. ZD2019008; ZD2019082).

References

Abu-Awwad A.M., (1999), Irrigation water management for efficient water use in mulched onion, *Journal of Agronomy and Crop Science*, **183**, 1-7.

Ajami H., Maddock T., Meixner T., Hogan J.F., Guertin D.P., (2012), RIPGIS-NET: A GIS tool for riparian groundwater evapotranspiration in MODFLOW, *Ground Water*, **50**, 154-158.

Barazzuoli P., Nocchi M., Rigati R., Salleolini M., (2008), A conceptual and numerical model for groundwater management: A case study on a coastal aquifer in southern Tuscany, Italy, *Hydrogeology Journal*, **16**, 1557-1576.

Berkoff J., (2003), China: The south–north water transfer project-is it justified?, *Water Policy*, **5**, 1-28.

Bietresato M., Mazzetto F. (2020), Morphometry as a key to investigate the stability to a wind-induced rollover of agricultural equipment for irrigation. *International Journal of Safety and Security Engineering*, **10**, 129-139.

Borgia A., Cattaneo L., Marconi D., Delcroix C., Rossi E.L., Clemente G., Amoroso C.G., Lo Re F., Tozzato E., (2011), Using a MODFLOW grid, generated with GMS, to solve a transport problem with TOUGH2 in complex geological environments: The intertidal deposits of the Venetian Lagoon, *Computers & Geosciences*, **37**, 783-790.

Brunner P., Simmons C.T., Cook P.G., Therrien R., (2010), Modeling surface water–groundwater interaction with MODFLOW: Some considerations, *Groundwater*, **48**, 174-180.

Bumb A.C., Mitchell J.T., Gifford S.K., (1997), Design of a ground-water extraction/reinjection system at a superfund site using MODFLOW, *Ground Water*, **35**, 400-408.

Clemo T., (2005), Improved water table dynamics in MODFLOW, *Ground Water*, **43**, 270-273.

Doble R.C., Simmons C.T., Walker G.R., (2009), Using MODFLOW 2000 to model ET and recharge for shallow ground water problems, *Ground Water*, **47**, 129-135.

Fu X.G., Tang Z.H., Lv W.B., Wang X.M., Yan B.Z., (2018), Exploitation potential of groundwater in Yangzhuang Basin, China under recharge enhancement, *International Journal of Heat and Technology*, **36**, 483-493.

Geng X.Y. (2020), On the regional differences in agricultural water use efficiency in China and their convergence, *International Journal of Design & Nature and Ecodynamics*, **15**, 189-196.

Geng Y., Ma J., Jia R., Xue L.Q., Tao C.J., Li C.J., Ma X.D., (2013), Impact of long-term atrazine use on groundwater safety in Jilin Province, China, *Journal of Integrative Agriculture*, **12**, 305-313.

Hanson R.T., Schmid W., Faunt C.C., Lockwood B., (2010), Simulation and analysis of conjunctive use with MODFLOW's farm process, *Ground Water*, **48**, 674-689.

Huo Z.L., Feng S.Y., Kang S.Z., Huang G.H., (2012), Integrated neural networks for monthly river flow estimation in arid inland basin of Northwest China, *Journal of Hydrology*, **420**, 159-170.

Jhorar R.K., Smit A.A.M.F.R.W., Bastiaanssen G.M., Roest C.W.J., (2011), Calibration of a distributed irrigation water management model using remotely sensed evapotranspiration rates and groundwater heads, *Irrigation and Drainage*, **60**, 57-69.

Kinzelbach W., Marburger M., Chiang W.H., (1992), Determination of groundwater catchment areas in two and three spatial dimensions, *Journal of Hydrology*, **134**, 221-246.

Kushwaha R.K., Pandit M.K., Goyal R., (2009), MODFLOW-based groundwater resource evaluation and prediction in Mendha sub-basin, NE Rajasthan, *Journal of the Geological Society of India*, **74**, 449-458.

Li Y.F., Song G.H., Wu Y.G., Wan W.F., Zhang M.S., Xu Y.J., (2009), Evaluation of water quality and protection strategies of water resources in arid-semiarid climates: A case study in the Yuxi River Valley of Northern Shaanxi Province, China, *Environmental Geology*, **57**, 1933-1938.

Lin L., Yang J.Z., Zhang B., Zhu Y., (2010), A simplified numerical model of 3-D groundwater and solute transport at large scale area, *Journal of Hydrodynamics*, **22**, 319-328.

Liu P.L., Fang Z., Lv C.Y., Ruan A.M. (2020), China's agricultural water-use efficiency and its influencing factors under the constraint of pollution emission. *International Journal of Design & Nature and Ecodynamics*, **15**, 579-585.

Liu X., (2005), The optimal allocation of water Jinghuiqu Canal Irrigation of Shaanxi Province, *Journal of Water Conservancy and Architectural Engineering*, **3**, 62-64.

Liu Y., Zhu H.Y., (2011), The water environment deterioration characteristics and groundwater regulation and storage capacity of Jinghuiqu irrigation district, *Transactions of the CSAE*, **27**, 19-24.

Maheswaran G., Elangovan K., (2010), Hydrogeochemical studies of groundwater in Salem District, Tamil Nadu (India), *Indian Journal of Environmental Health*, **52**, 47-52.

Odeh T., Mohammad A.H. (2020), Wise water resources management under the increasing number of refugees in the third poorest water resources country (Jordan) – a suggested future spatial plan for water resources investments. *International Journal of Sustainable Development and Planning*, **15**, 235-238.

Pathak D.R., Hiratsuka A., (2011), An integrated GIS-based fuzzy pattern recognition model to compute groundwater vulnerability index for decision making, *Journal of Hydro-Environment Research*, **5**, 63-77.

Praveena S.M., Aris A.Z., (2010), Groundwater resources assessment using numerical model: A case study in low-lying coastal area, *International Journal of Environmental Science & Technology*, **7**, 135-146.

Rushton K., (2010), Simulating piecewise-linear surface water and groundwater interactions with MODFLOW, *Ground Water*, **48**, 796-797.

Vovna O.V., Laktionov I.S., Dobrovolska L.O., Kabanets M.M., Lebediev V.A., (2019), Evaluation of metrological characteristics of a computerized conductivity meter of irrigation solution based on the uncertainty theory. *Journal Européen des Systèmes Automatisés*, **52**, 333-340.

Wang S., Huang G.H., (2011), Interactive two-stage stochastic fuzzy programming for water resources management, *Journal of Environmental Management*, **92**, 1986-1995.

Wang X.Q., Liu C.M., Zhang Y., (2002), A simultaneous approach to water-resource protection and economic structural adjustment-A case study of Guanzhong region in the Huanghe river basin, China, *Chinese Geographical Science*, **12**, 35-43.

Wang Z.N., Wang M.X., Hu X.T., Cao H.X., Shang H.J., Xue J.X., Xue D.W., Zhou A.L., (2003), Monitoring and evaluation networks for management system reform in Guanzhong Irrigation District of Shaanxi Province in China, *Journal of Experimental Botany*, **54**, 45-45.

Xiao F., Li Y.Z., Du Y., Ling F., Yan Y., Feng Q., Ban X., (2014), Monitoring perennial sub-surface waterlogged croplands based on MODIS in Jianghan plain, middle reaches of the Yangtze River, *Journal of Integrative Agriculture*, **13**, 1791-1801.

Xie W.P., Yang J.S., (2013), Assessment of soil water content in field with antecedent precipitation index and groundwater depth in the Yangtze river estuary, *Journal of Integrative Agriculture*, **12**, 711-722.

Xu X., Huang G.H., Qu Z.Y., (2009), Integrating MODFLOW and GIS technologies for assessing impacts of irrigation management and groundwater use in the Hetao Irrigation District, Yellow River basin, *Science in China Series E: Technological Sciences*, **52**, 3257-3263.

Xu X., Huang G.H., Qu Z.Y., Pereira L.S., (2011), Using MODFLOW and GIS to assess changes in groundwater dynamics in response to water saving measures in irrigation districts of the upper Yellow river basin, *Water Resources Management*, **25**, 2035-2059.

Zhang D.S., Zhang Y.X., Yang Y., Li B.H., Li Q., (2019), Numerical simulation of groundwater recharge from south-to-north water division project, *International Journal of Heat and Technology*, **37**, 188-196.

Zhao W.J., Ma X.Y., Zhang J.X., (2009), Impact of climate and discharge change on sustainable development in Jinghuiqu irrigation district and counter measures, *Journal of Natural Resources*, **24**, 1163-1170.